JOURNAL OF GEOPHYSICAL RESEARCH VOL. 69, NO. 21 NOVEMBER 1, 1964

Studies of Planetary Atmospheres

1. The Distribution of Electrons and Ions in the Earth's Exosphere

J. J. ANGERAMI AND J. O. THOMAS[1]

Radioscience Laboratory, Stanford University, Stanford, California

Abstract. The factors which govern the distribution of electrons and ions in a planet's exosphere under diffusive equilibrium are discussed. The theory takes into account the effect of the electric field that arises from charge separation, the centrifugal force arising from the rotation of the planet, and the effect of the planet's gravitational field. It is assumed that the charged particles are constrained to move only along the direction of the planet's magnetic lines of force. The modifications that result in the electron and ion distributions when a temperature variation is assumed along a line of force are also considered. The results predicted by the theory are compared with actual experimental observations of the electron density distribution in the earth's exospheric plasma which have been obtained in recent years from whistler data and from topside ionograms made by the Alouette satellite.

INTRODUCTION

A great deal of experimental data on the distribution of ions and electrons in the earth's upper ionosphere are becoming increasingly available as the new techniques required to investigate the physical properties of the exosphere at these heights are developed. An excellent brief report on experimental work in this field has been published recently by *Bordeau* [1963]. The basic theoretical concepts which govern the distributions of ions and electrons in the exosphere have been discussed in a number of important papers in the scientific literature. It is generally agreed that the main constituent of the atmosphere at great heights above the earth (above approximately 1500 km) is hydrogen. Hydrogen ions are formed by the reaction

$$O^+ + H \rightleftarrows H^+ + O$$

as *Dungey* [1954] first pointed out. The relative equilibrium concentrations in the exosphere are determined largely by the importance of this reaction near the base of the neutral particle exosphere where the cross section for collisions between ions and neutral particles is relatively high. The base of the exosphere (approximately 550 km) is believed to be the most probable level of origin for protons entering the exosphere from below after formation in the charge exchange reaction referred to above [*Johnson*, 1960]. Thus, the relative abundances of O^+ and H^+ (and also of the He^+ ions) at the base of the exosphere control the electron and ion distributions throughout the exosphere. The charge exchange reaction proceeds very rapidly near the peak of the F_2 layer, and the proton number density is given by the chemical equilibrium expression [*Hanson and Ortenburger*, 1961]

$$[H^+] = \frac{9}{8}\frac{[H][O^+]}{[O]}$$

where the square brackets denote the concentrations of the constituents bracketed.

Hanson and Ortenburger [1961] have also shown that the oxygen ions near the F_2 peak are only weakly coupled with the protons in the protonosphere, and it seems likely that the time constant for the establishment of equilibrium between the two hemispheres near the F-region peak is greater than one day. *Hanson and Patterson* [1963] and *Hanson et al.* [1963] provided an estimate of the proton fluxes likely to be involved as the result of the diurnal variation of the abundance of the atomic hydrogen in the exosphere. They considered the flow of hydrogen into and out of the protonosphere by

[1] Now at Ames Research Center, National Aeronautics and Space Administration, Moffett Field, California.

the charge exchange process referred to above, the escape of hydrogen from the daytime exosphere associated with higher daytime temperatures, and also the lateral flow of hydrogen around the earth due to any asymmetry in the distribution of hydrogen around the earth.

It is clear from this work and from other considerations that some modifications to a simple equilibrium theory are probably required to describe completely the physics of the exosphere in terms of diurnal and other changes. However, before a nonequilibrium theory is properly applied, it is valuable to explore the extent to which an equilibrium theory is adequate to explain the observational data, and this has been the purpose of the work reported herein. In particular, it seems likely that an equilibrium theory might be applicable for explaining seasonal variations which are likely to occur in a given hemisphere, as well as other changes involving time constants greater than one day.

In the first part of this paper the general theoretical considerations which govern the distribution under diffusive equilibrium of electrons and ions in a multiconstituent planetary exosphere in the presence of a magnetic field are discussed. These distributions are derived on the assumptions that the charged particles are constrained to move only along the direction of the magnetic lines of force under the action of the planet's gravitational field and of the centrifugal force arising from the rotation of the planet. The effect of the electric field E which arises from the charge separation that [*Mange*, 1960] results from the tendency of electrons to rise with respect to the heavier positive ions is also taken into account. The modifications that result in the electron and ion distributions when a temperature variation along a line of force is assumed, such that there are significant temperature differences between the northern and southern hemispheres near the base of the exosphere, are also considered. Special attention is given to the electron distributions that result when computed along a line of force ($N(s)$ curves) and to the resulting vertical profiles ($N(h)$ curves) calculated in the equatorial plane.

In the second part of the paper, the electron and ion distributions predicted by the theory for the terrestrial exosphere when certain reasonable assumptions are made about the physical properties of the earth's upper atmosphere are described. These are then compared both with experimental observations and with the theoretical predictions of a number of other workers, including *Dungey* [1954], *Johnson* [1960, 1962], and *Bates and Patterson* [1961], who have discussed the structure of the earth's upper exosphere; the structure of the earth's lower exosphere has been considered in some detail by *Hanson* [1962], *Bauer* [1962, 1963], and *Gliddon* [1963], who derived the distributions of O^+, He^+, and H^+ ions, together with the electrons under diffusive equilibrium.

The theory is applicable to any multiconstituent planetary atmosphere in diffusive equilibrium provided that the assumptions and restrictions described here are valid. For convenience, however, the theory is described, in what follows, in terms relating to the situation in the earth's atmosphere.

In the present work the following points are particularly emphasized:

1. Under the circumstances where diffusive equilibrium applies, it is well known that, whereas in a nonionized atmosphere each constituent is distributed independently of the other constituents, the distribution of a light ionic constituent in diffusive equilibrium *is* dependent on the presence of the others because of the electric field E which arises from the slight charge separation between electrons and positive ions [*Dungey*, 1954; *Mange*, 1960; *Hanson and Ortenburger*, 1961]. In the present work, it has been assumed that the electrons and ions can diffuse only along the geomagnetic field lines and, therefore, the direction of the electric field E has been assumed to be along the particular field line concerned.

2. It is convenient to work in terms of a parameter z, the temperature-modified geopotential height. This parameter takes into account the effect of the centrifugal and gravitational forces acting on a particle and also provides for the possibility that the electron and ion temperatures may be different and that a temperature gradient may exist along a line of force.

3. As *Bates and Patterson* [1961] first pointed out, up to the present time the theories of electron and ion distributions in the earth's exosphere have not taken into account condi-

tions in the upper part of the earth's ionosphere which may be strongly dependent on latitude. Such a latitude dependence would influence the electron density distribution in the equatorial plane, since the diffusion of charged particles in the earth's exosphere is appreciable only along geomagnetic field lines. Since our $N(h)$ profiles have been deduced from the theoretically computed $N(s)$ distributions (i.e., the calculated equilibrium distributions along a line of force when diffusion along the field lines is operative), the starting electron density, ionic composition, and temperature assumed at the base level and their variation with latitude are extremely important. In other words, the key factors in determining the electron density at a given altitude are not the magnitudes of the temperature or ionic relative abundances at the exospheric base level vertically beneath the point concerned, but are rather the magnitudes of these quantities at some higher latitude where the field line through the point intersects the critical level at the base of the exosphere.

The results of *Thomas and Sader* [1963, 1964] show that the electron density at 1000 km as observed by the Alouette satellite varies quite strongly with latitude and, in particular, that there is an important minimum in the curve under certain circumstances near a dip latitude of 65°. This latitude dependence was inserted into the theory, so that the actual observed electron densities at 1000 km were used. The computed $N(h)$ curves in the equatorial plane at great distances from the earth were then compared with observations from whistler data. It was found that the disagreement between earlier theoretical work and observations of the exospheric plasma electron density distribution in the vicinity of the Alouette orbit was removed, and the theory gives the correct slope for the $N(h)$ profile near the Alouette orbit, in agreement with the results of *Bauer* [1962, 1963].

It is well known that at the present time the theoretically predicted rate of decrease of electron density with altitude above about two earth radii does not agree with the observed rate in the equatorial plane, which is much greater. Under certain circumstances, this disagreement at greater distances from the earth is removed when reasonable assumptions about the exospheric temperature and about the relative ion densities at 500 km are made and the Alouette data for summer nights used.

Clearly, at the times when the observed $N(h)$ slopes far out do not agree with theory, some of the assumptions were probably invalid. In particular, it seems likely that the composition and temperature at 1000 km change with latitude, and it is also probable that the level above which diffusive equilibrium occurs varied with time.

The main conclusions of the paper are described and summarized in the last section. A more detailed account of the work described has been published recently as a technical report [*Angerami and Thomas,* 1963].

The Problem and the Assumptions

The electrons and ions in the earth's exosphere are acted upon by a number of important forces. These include the gravitational attraction toward the earth, the centrifugal force due to the rotation of the earth about its geographic axis, and the force due to the electric field E resulting from the tendency of electrons to rise with respect to the heavier positive ions [*Mange,* 1960]. In this region of space it is assumed that the particles are in diffusive equilibrium and obey Dalton's law of partial pressures, so that each constituent has a partial pressure corresponding to that which it would have if it were the only constituent present. The distribution of electrons and ions which would arise under these circumstances will be modified if there is a gradient of temperature along a line of force.

The main assumptions used in this analysis are listed below:

1. The upper atmosphere, above 500 km, consists of neutral particles together with a neutral mixture of singly charged positive ions and electrons only, and these are in diffusive equilibrium. The positive ions are O^+, He^+, and H^+, and their relative abundances at the base level at 500 km are assumed to be known.
2. The partial pressure for each species is balanced by the earth's gravitational and centrifugal forces and the force due to the electric field arising from charge separation.
3. The charged particles are constrained to move only along the lines of force of the earth's

magnetic field, so that the distributions along different lines of force are quite independent of each other.

4. No electrons are produced by the action of the sun's ionizing radiations above 500 km.

5. The rate at which electrons recombine is so small in comparison with other effects that the loss of electrons by this process can be neglected in the calculations.

6. The axis of rotation of the earth coincides with the magnetic dipole axis.

7. A difference of temperature can exist between the northern and southern hemispheres. The ratio of the temperatures in the southern and northern hemispheres, respectively, is not greater than 1.5, consistent with satellite drag observations of atmospheric densities [*King-Hele and Walker*, 1960].

The calculations described are aimed at deriving the resulting electron distributions along a line of force.

Nomenclature

The subscripts e and i denote electrons and ions, respectively, and the subscript 0 denotes values measured at the base level, usually taken to be 500 km above the earth.

C	Ratio of electron to ion temperature.
η	Electron density at 500 km relative to O^+ density at that level.
η_i	Ion density at 500 km relative to O^+ density at that level.
h	Altitude.
H_i	Scale height of nonionized ion at 500 km.
m_e	Electron mass.
m_i	Ion mass.
m_+	Temperature-weighted ion mass average.
n_e or N	Electron density.
n_{e0}	Electron density at the base level.
n_i	Ion density; $i = 1, 2, 3$, for O^+, He^+, and H^+, respectively.
n_{i0}	Ion density at the base level.
R_e	Ratio of electron densities at a fixed level at conjugate points in the two hemispheres.
$s(\theta_0, \theta)$	The distance measured along a line of force from its foot (at 500 km) to the point (θ_0, θ) on the field line.
$s'(\theta_0, \theta')$	The distance measured along a line of force from its foot (at 500 km) to the point (θ_0, θ'). It is used as an upper limit of integration.
$s_M(\theta_0)$	$\equiv s(\theta_0, 0)$.
$t(s)$	Ratio of electron or ith ion temperature at the base level to the corresponding temperature at the distance s along the line of force from the base level $(t(s) = T_{e0}/T_e(s) = T_{i0}/T_i(s))$.
T	Electron or ion temperatures when they are assumed to be the same in an isothermal exosphere.
T_e	Electron temperature.
T_{e0}	Electron temperature at 500 km.
T_i	Ion temperature.
T_{i0}	Ion temperature at 500 km.
T_0	Electron or ion temperature at 500 km when they are assumed to be equal.
$T(s)$	Electron or ion temperatures when they are assumed to be equal.
θ	Geomagnetic latitude of a point on a field line.
θ_0	Geomagnetic latitude of a field line at 500 km above the earth's surface.
θ'	Geomagnetic latitude of a point on a field line when this point is the upper limit of an integration.
(θ_0, θ)	Coordinates of a point on a magnetic field line in terms of the latitude θ of the point and the latitude θ_0 of the foot (at 500 km) of the particular field line concerned.
$z(\theta_0, \theta')$	Temperature-modified geopotential height, corresponding to the point (θ_0, θ'). For an isothermal exosphere, z is sometimes referred to as the geopotential height.

Theoretical Formulation of the Solution

Force on Unit Mass

The total force $\mathbf{g}$ acting on a unit mass at a point A, represented by the coordinates (r, θ), (θ_0, θ), or (θ_0, s) (Figure 1), is given by

$$\begin{aligned}\mathbf{g}(r, \theta) &= \mathbf{f}_g(r, \theta) + \mathbf{f}_c(r, \theta) \\ &= -\mathbf{u}_r g_0(r_0^2/r^2) + \mathbf{u}_x \Omega^2 r \cos\theta\end{aligned} \tag{1}$$

where $\mathbf{g}_0$ is the total force on a unit mass at the reference level r_0 at the poles, Ω is the angular velocity of rotation of the earth about the geographic axis, $\mathbf{f}_g$ and $\mathbf{f}_c$ are the gravitational

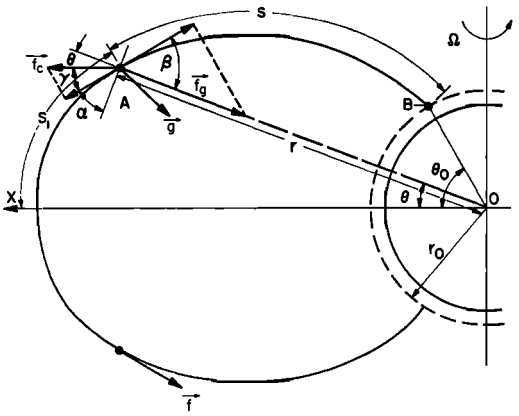

Fig. 1. Gravitational and centrifugal forces (f_g and f_c) acting on unit mass located at the point A defined by one of the coordinate pairs (r, θ), (θ_0, θ), or (θ_0, s).

and centrifugal forces, respectively, $\mathbf{u}_r$ and $\mathbf{u}_x$ are unit vectors in the directions of r and x, respectively, and the distance s is measured along a line of force (Figure 1).

The magnitudes of $\mathbf{f}_g$ and $\mathbf{f}_c$ and the resultant force $\mathbf{g}(r, \theta)$ acting on a unit mass are drawn to scale in Figure 2 for different positions along the line of force through 70° geomagnetic latitude. If it is assumed that charged particles can move only along the lines of force of the magnetic field, it becomes important to consider the variation in space of the resultant force $\mathbf{f}(r, \theta)$ obtained by considering only the resolved component of $\mathbf{g}(r, \theta)$ along the direction of the earth's lines of force. The loci of points at which $\mathbf{f}(r, \theta)$ is zero are shown as the broken curves (CD) in Figure 2. Referring to Figure 1 and (1), it is clear that the algebraic value of this force f is given by

$$f(r, \theta) = g_0(r_0^2/r^2) \cos \beta - \Omega^2 r \cos \theta \cos \gamma \quad (2)$$

From Figure 1 it can be shown that

$$\cos \beta = \sin \alpha = \frac{2 \tan \theta}{\sqrt{1 + 4 \tan^2 \theta}} \quad (3a)$$

$$\cos \gamma = \sin (\alpha + \theta) = \frac{3 \sin \theta}{\sqrt{1 + 4 \tan^2 \theta}} \quad (3b)$$

where α is the magnetic dip at (r, θ) given by

$$\tan \alpha = 2 \tan \theta$$

Substituting the above values in (2), changing the variables (r, θ) to (θ_0, θ), where θ_0 is the dipole latitude at the reference level r_0, and using (A.1) of appendix A:

$$f(\theta_0, \theta) = \frac{\sin \theta}{\sqrt{1 + 4 \tan^2 \theta}} \cdot \left(2g_0 \cos^4 \theta_0 \frac{1}{\cos^5 \theta} - \frac{3\Omega^2 r_0}{\cos^2 \theta_0} \cos^3 \theta \right) \quad (4)$$

Equation 4 gives the resultant force resolved along the direction of the earth's magnetic field line, arising from the combined action of the earth's centrifugal and gravitational forces. It is clearly a function of the geomagnetic latitude θ_0 at which the line of force under consideration crosses the reference level and of the distance from the earth's surface to the point under consideration as represented by the coordinate θ, Figure 1.

Derivation of Equilibrium Distributions

There is strong evidence, both theoretical [*Nicolet*, 1961] and experimental [e.g., *Hanson*, 1962], for supposing that the main ionized constituents of the upper atmosphere above the peak of the F_2 layer are electrons, together with oxygen, helium, and hydrogen ions in the atomic state. In the analysis below, it is assumed that these are the only ionized constituents and that no negative ions or doubly charged positive ions are present. The ions will be referred to by subscript i and electrons by subscript e. It is assumed that the lines of force act as barriers across which charged particles cannot flow.

Assuming (Figure 3) that the pressure changes

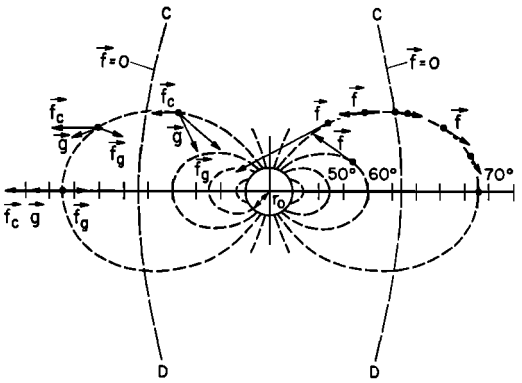

Fig. 2. The relative magnitudes of the gravitational and centrifugal forces at different points along a line of force.

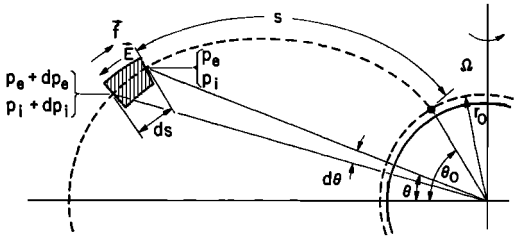

Fig. 3. To illustrate an element of volume taken along a line of force. The partial pressures of the ions and electrons, p_i and p_e, and the electric field E [*Mange*, 1960] are also shown.

by an amount dp over the distance ds measured along the line of force, we can write

$$\begin{aligned} dp_e &= -m_e n_e f\, ds - n_e eE\, ds \\ dp_i &= -m_i n_i f\, ds + n_i eE\, ds \end{aligned} \tag{5}$$

where the field E, directed as shown in Figure 3, arises from the small separation between charges due to the fact that electrons are lighter than the positive ions and, therefore, tend to move upward [*Mange*, 1960]. In these equations, m_e and m_i are the mass of the electron and of the ith ion, n_e and n_i are the electron and ith ion densities, e is the electronic charge, and p_e and p_i represent the partial pressures of the electrons and the ith ions, respectively.

It should be noted that the gradient of partial pressure of the electrons changes direction according to whether the point under consideration is inside or outside the lines CD in Figure 2. From Dalton's law for the partial pressures of the constituents of a gas in diffusive equilibrium, we know that each constituent, in this case each ion species and the electrons, has a partial pressure corresponding to that which it would have if it were the only constituent present. We can then write

$$p_e = n_e k T_e \qquad p_i = n_i k T_i \tag{6}$$

where T_e and T_i refer to the electron and ion temperatures, respectively, and in the subsequent theory it is assumed that these can be different. Since the atmosphere at every point is taken to be electrically neutral, we can write

$$dp_e/T_e = \sum_i dp_i/T_i \tag{7}$$

provided that

$$T_e(s)/T_i(s) = C_i \tag{8}$$

where C_i is not a function of s.

Equation 8 implies that the ion and electron temperatures vary together with s:

$$\frac{T_{e0}}{T_e(s)} = \frac{T_{i0}}{T_i(s)} = t(s) \quad \text{say} \tag{9}$$

Using (5) and (7) and noting that $m_i \geq 1836 m_e$ and $C_i \geq 1$, we can show that the electric field is given by

$$eE = \left\{ \frac{2 \sum_i m_i n_i C_i}{\sum_i n_i (C_i + 1)} \right\} \frac{f}{2} = \frac{m_+}{2} \cdot f \tag{10}$$

where m_+, the quantity in brackets, can be called the 'temperature-weighted ion mass average.' Combining (5), (6), and (10)

$$\begin{aligned} \frac{d(n_e T_e)}{n_e T_e} &= -\frac{m_+}{2kT_e} f\, ds \\ \frac{d(n_i T_i)}{n_i T_i} &= -\frac{[m_i - (m_+/2)]}{kT_i} f\, ds \end{aligned} \tag{11}$$

Equations 11 have a number of important consequences; if a constant temperature is assumed along a line of force for both the electrons and ions, they show that, above the reference level:

1. Since m_+ is always greater than zero, the electron density decreases with s and thus also with height.
2. If $m_i > m_+/2$, the ion density n_i decreases with s and thus with height. This condition is always satisfied by the heaviest constituent and also by a light constituent if it, or a still lighter one, is strongly predominant (see Figures 4 and 5).
3. If $m_i < m_+/2$, the ion density n_i increases with s and thus with height. This happens with a light constituent in the presence of a predominant heavier one.
4. If $m_i = m_+/2$, the ion density of constituent i (cannot be the heaviest) passes through a maximum.

Equations 11 are basic and contain the essential information about the distribution of both electron and ion densities with height. Integrating (11), the electron and ion densities at the point A at a distance s' measured along the line of force from the reference level r_0 (Figure 1) are given by

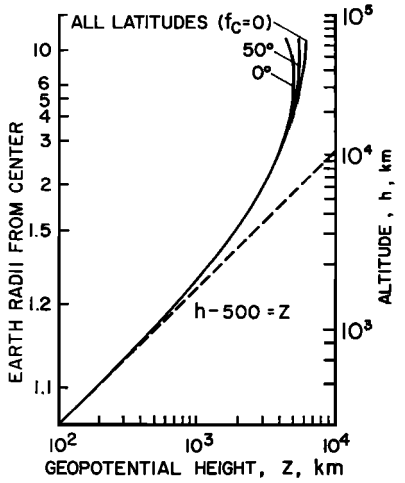

Fig. 4. Variation of the temperature-modified geopotential height z with altitude h. The electron and ion temperatures are each assumed constant along a field line, but they need not be equal in value.

$$\frac{n_e(s')T_e(s')}{n_{e0}T_{e0}} = \exp\left[-\int_0^{s'} \frac{m_+}{2kT_e} f\, ds\right] \tag{12}$$

$$\frac{n_i(s')T_i(s')}{n_{i0}T_{i0}} = \exp\left[-\int_0^{s'} \frac{[m_i - (m_+/2)]}{kT_i} f\, ds\right]$$

in which the electron and ion temperatures must be given as functions of s.

In the above integrals it is convenient to separate the effects of T and f as follows:

$$\int_0^{s'} \frac{m_+}{2kT_e} f\, ds = \int_0^{s'} \frac{m_+ g_0}{2kT_{e0}} \left\{\frac{f}{g_0}\frac{T_{e0}}{T_e}\right\} ds = \frac{g_0}{2kT_{e0}} \int_0^z m_+\, dz \tag{13a}$$

Similarly,

$$\int_0^{s'} \frac{[m_i - (m_+/2)]}{kT_i} f\, ds = \frac{g_0}{kT_{i0}} \int_0^z \left(m_i - \frac{m_+}{2}\right) dz \tag{13b}$$

In these equations, z is the 'temperature-modified geopotential height,' defined by

$$z = \int_{s=0}^{s=s'} \frac{f(s)}{g_0} t(s)\, ds \tag{14}$$

It should be noted that z is not the same as the quantity z used by *Bauer* [1962], but contains a dependence on the centrifugal force and on the temperature variation along a line of force. If the centrifugal force is zero and if $T_e = T_{e0}$ ($T_i = T_{i0}$, i.e., no temperature variation along the line of force, although the electrons and ions may have different temperatures), then our z reduces to Bauer's z. The calculation of the temperature-modified geopotential height z is discussed in appendix B. Its variation with altitude is shown in Figure 4 for different latitudes.

Equations 12 can now be written in terms of the temperature-modified geopotential height z as

$$n_e(s') = n_{e0}t(s') \cdot \exp\left[-\frac{g_0}{2kT_{e0}} \int_0^z m_+\, dz\right] \tag{15a}$$

$$n_i(s') = n_{i0}t(s') \exp\left[-\frac{z}{H_i}\right] \cdot \exp\left[\frac{g_0}{2kT_{i0}} \int_0^z m_+\, dz\right] \tag{15b}$$

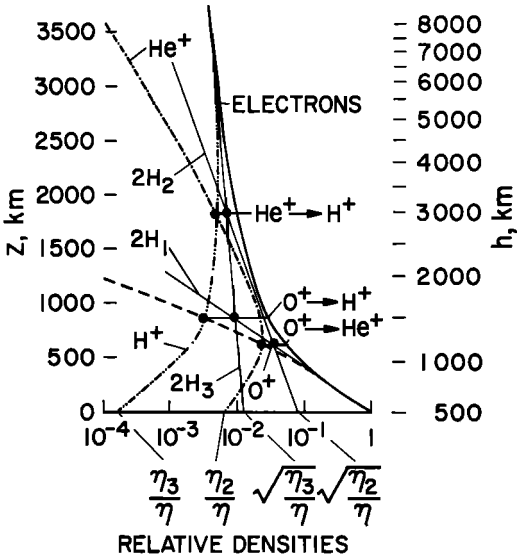

Fig. 5. Relative electron and ion densities *along a line of force* as a function of the temperature-modified geopotential height z for a constant temperature (1500°K). The vertical altitude scale h to each point on the line of force is derived from Figure 4. The electrons and ions are assumed to be at the same temperature ($C = 1$), and the ionic composition at the base level is given by $\eta_2 = 6.3 \times 10^{-5}$, $\eta_3 = 1.6 \times 10^{-4}$.

where

$$H_i = kT_{i0}/m_i g_0 \tag{16}$$

is the scale height of the nonionized atomic species i at the reference level.

From charge neutrality and (8) and (15a, b) we obtain

$$\frac{n_e(s')}{n_{e0}} = \frac{1}{n_{e0}} \sum_i \left\{ n_{i0} t(s')^{1+C_i} \cdot \exp\left(-\frac{z}{H_i}\right)\left(\frac{n_{e0}}{n_e(s')}\right)^{C_i} \right\} \tag{17}$$

Normalizing the ion densities at the reference level to the value for the heaviest ion (O^+), we write

$$\eta = \frac{n_{e0}}{n_{10}} = \sum_i \eta_i = \eta_1 + \eta_2 + \eta_3$$

where

$$\begin{aligned} \eta_1 &= 1 \\ \eta_2 &= n_{20}/n_{10} \\ \eta_3 &= n_{30}/n_{10} \end{aligned} \tag{18}$$

so that η is the electron density divided by the oxygen ion density at the reference level.

Equation 17 becomes

$$\frac{n_e(s')}{n_{e0}} = \frac{1}{\eta} \sum_i \left\{ \eta_i t(s')^{1+C_i} \cdot \exp\left(-\frac{z}{H_i}\right)\left(\frac{n_{e0}}{n_e(s')}\right)^{C_i} \right\} \tag{19}$$

In this equation, the first three factors in the summation are known, and the equation must be solved for $(n_e(s')/n_{e0})$.

If the ratios of ion temperature to electron temperature at the reference level are the same for all ions, that is

$$C_i = \frac{T_{e0}}{T_{i0}} = C \qquad i = 1, 2, 3 \tag{20}$$

then (19) becomes

$$\frac{n_e(s')}{n_{e0}} = t(s') \cdot \left\{ \frac{1}{\eta} \sum_i \left[\eta_i \exp\left(-\frac{z}{H_i}\right) \right] \right\}^{1/(1+C)} \tag{21}$$

Using (15a, b) and (20), we find the ion densities:

$$\frac{n_i(s')}{n_{i0}} = t(s')^{C+1} \exp\left(-\frac{z}{H_i}\right)\left\{\frac{n_{e0}}{n_e(s')}\right\}^C \tag{22}$$

The ion densities may also be referred to the electron density at the reference level with (18), so that

$$\frac{n_i(s')}{n_{e0}} = \frac{\eta_i}{\eta} t(s')^{C+1} \exp\left(-\frac{z}{H_i}\right)\left\{\frac{n_{e0}}{n_e(s')}\right\}^C \tag{23}$$

The distributions of electrons and ions in the exosphere are given by (21) and (23) in terms of the variable z, the temperature-modified geopotential height defined by (14). These equations provide the information we need to get the distribution of electrons and ions along a line of force and, hence, vertical profiles. It is shown in a later section that these general solutions reduce to the equations given by *Bauer* [1962] for the particular case he considered, i.e. the base of the terrestrial exosphere. The derived distribution equations 21 and 23 are discussed in detail below.

Form of Solution for Equilibrium Ion and Electron Densities

For the case in which the ion and electron temperatures are equal at the reference level (and hence, elsewhere, through equations 8) we have $C = 1$, and (21) becomes

$$\frac{n_e(s')}{n_{e0}} = t(s')\left\{\frac{1}{\eta} \sum_i \left[\eta_i \exp\left(-\frac{z}{H_i}\right) \right]\right\}^{1/2} \tag{24}$$

If the electron temperature is, say, twice the ion temperature, the exponent becomes 1/3.

From (23) the ratio of densities of two ions is

$$\frac{n_i}{n_j} = \frac{\eta_i}{\eta_j} \exp\left(z \frac{H_i - H_j}{H_i H_j}\right) \tag{25}$$

The ion densities will be equal at a value of $z = z_{ij}$ defined by

$$z_{ij} = \frac{H_i H_j}{H_i - H_j} \ln \frac{\eta_j}{\eta_i} \tag{26}$$

Since the subscripts 1, 2, and 3 refer, respectively, to O^+, He^+, and H^+, the scale heights are

$$H_2 = 4H_1 \qquad H_3 = 16H_1 \tag{27}$$

Hence, the values of z at which $n_1 = n_2$, $n_1 = n_3$, and $n_2 = n_3$ are, respectively, from (26):

$$z_{12}(O^+ \rightarrow He^+) = -\tfrac{4}{3}H_1 \ln \eta_2 \quad >0 \text{ if } \eta_2 < 1$$

$$z_{13}(O^+ \rightarrow H^+) = -\tfrac{16}{15}H_1 \ln \eta_3 \quad >0 \text{ if } \eta_3 < 1 \qquad (28)$$

$$z_{23}(He^+ \rightarrow H^+) = -\tfrac{16}{3}H_1 \ln (\eta_3/\eta_2) \quad >0 \text{ if } \eta_3 < \eta_2$$

Thus, two ions will have the same density at some height above the reference level if, at the reference level, the heavier one is more abundant. Also, from (26), at z greater than z_{ij}, the ion i will have higher density than the ion j if it is lighter. Therefore the z_{ij} defined by (28) are called transition values of z, and these are indicated in the same equations.

It is interesting to consider the conditions for which the transition $He^+ \rightarrow H^+$ happens above the transition $O^+ \rightarrow He^+$. From (28) this condition is

$$\eta_2 > \eta_3^{0.8} \qquad (29)$$

The distribution of electron density as a function of z (equation 21) can thus be written, using (27),

$$\frac{n_e(s')}{n_{e0}} = t(s')\left\{\frac{\exp(-x) + \eta_2 \exp(-x/4) + \eta_3 \exp(-x/16)}{\eta}\right\}^{1/(1+C)} \qquad (30)$$

where

$$x = z/H_1 \qquad (31)$$

If the reference level is low enough so that O^+ is strongly predominant there, then $\eta_2 \ll 1$ and $\eta_3 \ll 1$. For low values of x the exponentials in (30) are close to unity, and

$$\frac{n_e(s')}{n_{e0}} \simeq t(s') \exp\left(-\frac{x}{1+C}\right) \qquad (32)$$

Thus, apart from the factor $t(s')$, the electron density varies exponentially in z with scale height $(1 + C)H_1$.

For large values of x the first two exponentials in (30) become much smaller than the third, so that they can be disregarded and

$$\frac{n_e(s')}{n_{e0}} \simeq t(s')\left(\frac{\eta_3}{\eta}\right)^{1/(1+C)} \cdot \exp\left(-\frac{x}{16(1+C)}\right) \qquad (33)$$

Apart from the factor $t(s')$, the electron density presents, as a function of z, an exponential behavior with scale height $(1 + C)H_3$ and an asymptotic value

$$(\eta_3/\eta)^{1/(1+C)}$$

for $z = 0$.

Ion Distribution Curves in an Isothermal Exosphere

For an isothermal exosphere, the relative electron and ion densities can be conveniently plotted as functions of z. Assuming that the electrons and ions all have the same temperature (i.e., $C = 1$), their relative densities are obtained from (21), (22), and (23).

$$\frac{n_e(z)}{n_{e0}} = \left\{\frac{\exp(-z/H_1) + \eta_2 \exp(-z/H_2) + \eta_3 \exp(-z/H_3)}{\eta}\right\}^{1/2} \qquad (34)$$

$$\frac{n_i(z)}{n_{i0}} = \exp\left[-\frac{z}{H_i}\right]\left[\frac{n_{e0}}{n_e(z)}\right] \qquad (35)$$

$$\frac{n_i(z)}{n_{e0}} = \frac{\eta_i}{\eta} \exp\left[-\frac{z}{H_i}\right]\left[\frac{n_{e0}}{n_e(z)}\right] \qquad (36)$$

These equations can be compared with *Bauer*'s [1962], though his parameter z does not include the effect of the centrifugal force.

These equations have been used to compute the electron and ion distributions for a wide variety of assumed exospheric temperatures and assumed base compositions. The results have been presented in a series of curves by *Angerami and Thomas* [1963, Figures 4 and 9*a–e*]. A typical example, calculated for $T = 1500°K$, $\eta_2 = 6.3 \times 10^{-3}$, $\eta_3 = 1.6 \times 10^{-4}$, is shown in Figure 5.

If one ion is strongly predominant, so that only the term for this particular ion is important on the right-hand side of (34), then

$$\frac{n_e(z)}{n_{e0}} \simeq \sqrt{\frac{\eta_i}{\eta}} \exp\left[-\frac{z}{2H_i}\right] \qquad (37)$$

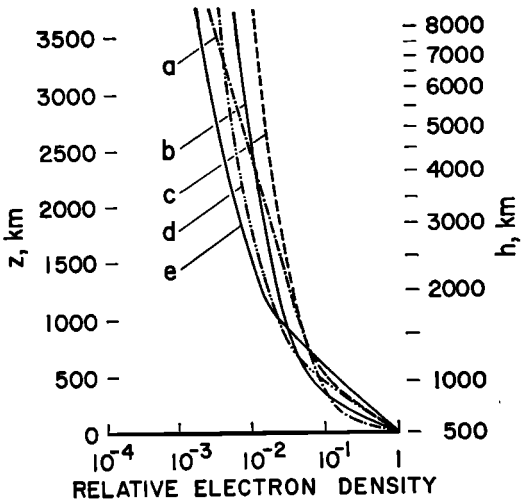

Fig. 6. Relative electron density *along a line of force* as a function of the temperature-modified geopotential height z for isothermal exospheres. The vertical altitude scale h to each point on the line of force is derived from Figure 4. The compositions at the base level and the temperatures corresponding to curves *a–e* are shown in Table 1.

where the subscript i refers to the strongly predominant ion. Equation 37 is a simple exponential and is represented by a straight line on semilogarithmic paper with slope $2H_i$ (twice the scale height of the nonionized specimen). These straight lines are drawn in Figure 5 for O^+, He^+, and H^+ [cf. *Hanson*, 1962] and are labeled $2H_1$, $2H_2$, and $2H_3$, respectively.

The $N(z)$ curve of Figure 5 shows that the simple exponential behavior of electron density referred to above is exhibited below $z = 200$ km where O^+ is strongly predominant and is also exhibited above $z = 3000$ km where H^+ is predominant. Around 1000 km, although He^+ is predominant, it is not sufficiently predominant, and a straight line distribution is not achieved. In Figure 6 the electron distributions shown in the quoted figures in *Angerami and Thomas* [1963] are drawn on one diagram for comparison purposes, the corresponding sets of ion density curves for each profile being omitted. The associated temperature and composition parameters are listed in Table 1.

Comparison of curves *c* and *d*, Figure 6, shows the effect in the slope of the $N(z)$ curve of changing the composition at the base level. According to Table 1, curve *d* of Figure 6 corresponds to a smaller percentage of He^+ and H^+ at the base level, so that the O^+ is predominant over a greater height range. Thus, the electron density maintains a high rate of decrease over a greater height range, so that the electron density turns out to be smaller for the same z in curve *d* than in curve *c*. As a result, we see that a change in composition is far more important than a change in temperature in determining the value of the relative electron density as a function of z. The distributions shown in Figure 6 do not show marked 'kinks' or cusps, and the ion transition levels do not show up clearly in the electron density curves.

These curves are discussed in greater detail in the next section.

In (35), the term $\exp(-z/H_i)$ decreases with increasing z, whereas the term $n_{e0}/n_e(z)$ increases with increasing z. It is therefore possible for the ion density to increase with z, since it is made up of the product of these two factors.

Equation 36 can be written in a more convenient form:

$$\left\{\frac{n_i(z)}{n_{e0}}\right\}\left\{\frac{n_e(z)}{n_{e0}}\right\} = \frac{\eta_i}{\eta}\exp\left[-\frac{z}{H_i}\right] \qquad (38)$$

so that the geometric mean of the electron and ith ion densities relative to the electron density at the base level is

$$\sqrt{\frac{\eta_i}{\eta}}\exp\left[\frac{-z}{2H_i}\right]$$

which is the previous (37) giving the asymptotic behavior for the relative electron density curve when the ith ion is strongly predominant. Thus from (38)

$$\frac{1}{2}\left\{\log\left[\frac{n_i(z)}{n_{e0}}\right] + \log\left[\frac{n_e(z)}{n_{e0}}\right]\right\} = \log\left\{\sqrt{\frac{\eta_i}{\eta}}\exp\left[\frac{-z}{2H_i}\right]\right\}$$

The left-hand side of this equation is the arithmetic mean of the logarithms of the electron density and the density of the ith ion relative to the electron density at the base level.

Thus, if relative electron density curves are plotted using a logarithmic scale in density (as in Figure 5), the distribution curve for the ion i can be derived from a simple geometric construction as follows. First the straight line (37) is plotted (slope $2H_i$, crossing the abscissa at a

TABLE 1. Data for the $N(z)$ Curves

Curve	T, deg K	η_2	η_3
a	500	6.3×10^{-2}	1.6×10^{-2}
b	1000	2.0×10^{-2}	1.6×10^{-3}
c	1500	2.0×10^{-2}	1.6×10^{-3}
d	1500	6.3×10^{-3}	1.6×10^{-4}
e	2000	2.0×10^{-3}	1.6×10^{-5}

value $(\eta_i/\eta)^{1/2}$), then the relative electron distribution (34) is plotted. For each value of z, a point is plotted such that the horizontal distance from the point to the straight line is the same as that from the straight line to the electron distribution. The locus of these points is the ion distribution curve (Figure 5). This procedure can be repeated for each ion.

It is clear from this construction that the ionic transition levels (the values of z at which two ions have the same density, i.e., the intersection point of two ionic distribution curves) can be alternatively identified as the intersection of the corresponding asymptotic straight lines.

Results of the Theory

Introduction

In this section, relative electron and ion density distributions calculated on the basis of the theory outlined in the preceding sections are presented. The results are given as distributions calculated as functions of the temperature-modified geopotential height z, as functions of the distance s measured along a line of force, and as functions of the altitude h. These distributions are referred to as $N(z)$, $N(s)$, and $N(h)$ curves, respectively. The computations are based on a number of different assumptions about the exospheric temperature and about the ionic composition of the atmosphere at 500 km. In particular, the distributions are derived (A) when a constant temperature is assumed along a line of force, and (B) when the temperature is assumed to vary with distance s along a line of force.

In addition, two sets of assumptions are made about the composition at the base level, usually taken to be 500 km above the earth's surface. These are (1) that the composition at 500 km is independent of the temperature at that level, and (2) that the composition at 500 km is a strong function of the temperature at that level.

The $N(h)$ curves are calculated both with a proper allowance for the effect of the centrifugal force arising from the earth's rotation and with this force neglected. Subsequently, observational data from the Alouette satellite [*Thomas and Sader*, 1963, 1964] are used to convert the relative electron density profiles into absolute profiles based on the electron density observed at approximately 1000 km. This leads to a set of theoretical profiles calculated on the basis of reasonable experimentally obtained magnitudes for ion composition [*Bauer*, 1963], temperature [*Harris and Preister*, 1962], and electron density at 1000 km (Alouette observations). These theoretical profiles are then compared with a number of whistler and other observations of electron density in the earth's exosphere. Tables 1 and 2 present the parameters used in the calculations. Typical results of the computations are presented below; a more

TABLE 2. Temperature and Composition Assumptions

Assumptions about Temperature	Assumptions about Composition at 500 km: Composition 1		Compositions 2: η_2	Compositions 2: η_3
A (T = constant)	$\eta_2 = 2.0 \times 10^{-2}$, $\eta_3 = 1.6 \times 10^{-3}$	2*a*. T = 500°K	6.3×10^{-2}	1.6×10^{-2}
		2*b*. T = 750	3.6×10^{-2}	5.1×10^{-3}
		2*c*. T = 1250	1.1×10^{-2}	5.1×10^{-4}
		2*d*. T = 1500	6.3×10^{-3}	1.6×10^{-4}
		2*e*. T = 2000	2.0×10^{-3}	1.6×10^{-5}
B, ($T = T(s)$)		2*f*. T_0 = 1400	8.0×10^{-3}	2.6×10^{-4}

complete set of results has been presented in the report by *Angerami and Thomas* [1963].

Electron and Ion Distributions

The electron and ion distributions presented below were calculated with a digital computer program. The $N(z)$ curves were computed from (34) on the assumption that the temperature was constant; the $N(s)$ curves were computed from (24), (A.4), and (B.4); the $N(h)$ profiles were subsequently computed from the $N(s)$ profiles using electron densities observed at 1000 km by Alouette.

The calculations in which the temperature is assumed constant along the line of force of the earth's magnetic field are denoted by the letter A (Table 2). For each temperature assumed, it is necessary to specify the composition at the base level (500 km). This composition was taken from the data presented by *Bauer* [1963] for the helium and hydrogen ion densities relative to the oxygen ion density as a function of temperature. The relevant equations are

$$\eta_2(T_0) = 0.2 \times 10^{-T_0/1000}$$
$$\eta_3(T_0) = 0.16 \times 10^{-T_0/500} \qquad (39)$$

In this equation, T_0 is the temperature assumed at the reference level. The variation of η_2 and η_3 with temperature, as given by (39), is shown in Figure 7.

The exospheric temperature enters the calculations in three ways: first, via the temperature-modified geopotential height z; second, via the scale heights H_i; and third, via its effect on the composition assumed at the base level through (39). It is interesting, however, to carry out computations in which the composition at 500 km is held constant while the temperature is allowed to vary. In this case the values for η_2 and η_3 are taken from (39) using $T_0 = 1000°K$; these results are referred to as 'composition 1' in Table 2.

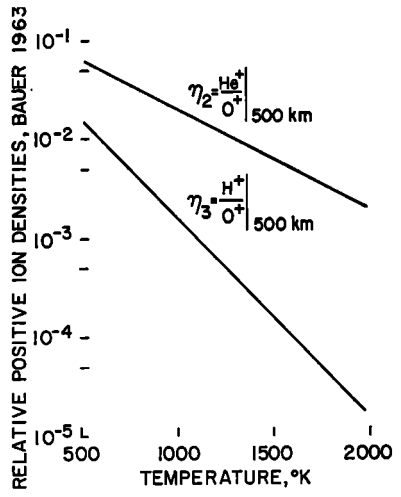

Fig. 7. Variation of the ion composition at 500 km with the temperature at that level [*Bauer*, 1963].

The calculations in which (39) was applied to give the relative densities at 500 km are referred to as 'compositions 2*a*, *b*, *c*,' etc., depending on the value of the temperature at 500 km (see Table 2). Some calculations were also performed using the assumption that the temperature is changing along the field line. These results, denoted by the letter B (Table 2), will be described later.

A comparison of the electron density curves of Figure 6 indicates the relative effects of temperature and composition changes on the computed profiles. At low values of z, where O^+ is predominant for all curves, the slopes are proportional to temperature. As we go to higher values of z the effect of the ion composition at the base becomes relatively more important, and the slopes are no longer simply proportional to temperature. For instance, at $z = 3000$ km the slope of curve e (2000°K) is less than the slope of curve b (1000°K). This is so because, although for curve b at $z = 3000$ km the H^+ is strongly predominant, it is not for curve e.

An examination of the curves of Figures 5 and 6 shows that the ion transition levels (the levels at which $n(O^+) = n(He^+)$, etc.) change with temperature (see equations 28). The variation of the ion transition levels with temperature is shown in Figure 8 for two different assumptions about the composition at the base level, namely, that the composition is independent of temperature (continuous lines) and that the composition is temperature-dependent, as indicated by (39) (broken lines). An important conclusion that can be drawn from Figure 8 is that the transition levels approach nearer the earth at night. These curves agree with those given by *Bauer* [1963].

The $N(z)$ curves of Figure 6 can be transformed using (B.4) into curves giving N as a

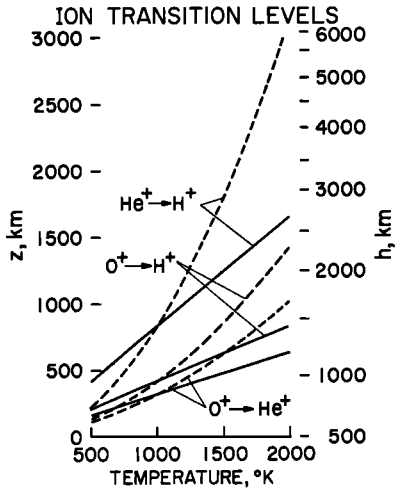

Fig. 8. The variation with temperature of the levels at which the ions indicated have equal abundances. The broken lines correspond to the cases when the composition at the base level depends on the temperature there (through equations 39). The continuous lines correspond to the case when the composition at the base level is independent of temperature (composition 1). These results are in agreement with those presented earlier by *Bauer* [1963]. They apply to the case $C = 1$.

function of θ and θ_0, where θ is the angle between the equatorial plane and a point at a distance s measured along a field line. The field line is assumed to intersect the base level (500 km above the earth) at a point making an angle θ_0 with the equatorial plane (Figure 1). The use of (A.4), appendix A, converts the $N(\theta, \theta_0)$ curves to distributions of electron density along a line of force ($N(s, \theta_0)$ curves). Examples of curves of this kind are given in Figure 9 for $\theta_0 = 55°$. In this figure, the results corresponding to the case in which proper allowance has been made for centrifugal force are shown as continuous lines. The corresponding results for the cases in which the centrifugal force was neglected are shown by broken lines. As was expected, the effect of the centrifugal force is largest at the higher altitudes, and tends to increase the electron density at the high levels. The increase is never greater than about 20% over the range of heights considered. It is found also that inclusion of the centrifugal force has no appreciable effect for $\theta_0 < 45°$. The effects of changes in temperature and composition are also seen in Figure 9.

Similar calculations (denoted by the letter B, Table 2) were carried out in which the temperature varied along a line of force. The temperature distribution assumed along a line of force in the cases labeled B is given by the formula

$$T(s) = T_0 + (T_T - T_0) \cdot \frac{1 - \exp(-s/D)}{1 - \exp(-s_M/D)} \qquad (40)$$

where T_0 is the temperature at the reference level (500 km), T_T is the temperature at the top of the field line, D is a variable distance along the line of force (taken to be 10^4 km), and the distances s and s_M are defined along the line of force as indicated in Figure 10. The variation of temperature with distance along a line of force $T(s)$ is sketched in Figure 11.

Relative electron densities along lines of force were calculated by means of (24), (A.4), and (B.3). Typical results are shown in Figure 12 for $\theta_0 = 55°$ (Table 2). The general behavior of these curves is similar to that of the curves in Figure 9. For instance, increasing temperature, while keeping the base level composition constant, increases the electron densities in both cases, and a contrary effect is produced if the composition is supposed to vary as given by

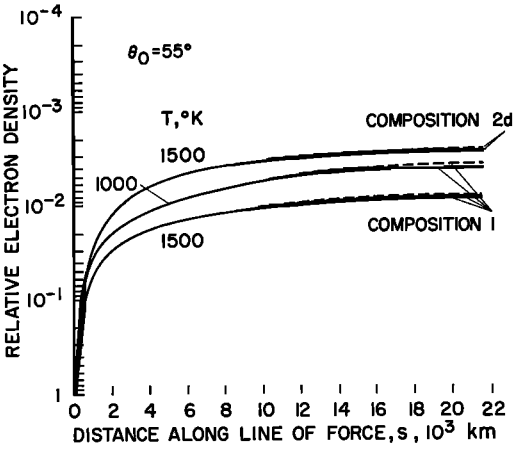

Fig. 9. The relative electron density distributions along a field line with feet (at 500 km above the earth) at geomagnetic latitude 55° (see Table 2) for an isothermal exosphere. The broken lines indicate the distributions that would have been obtained if the centrifugal force had been neglected.

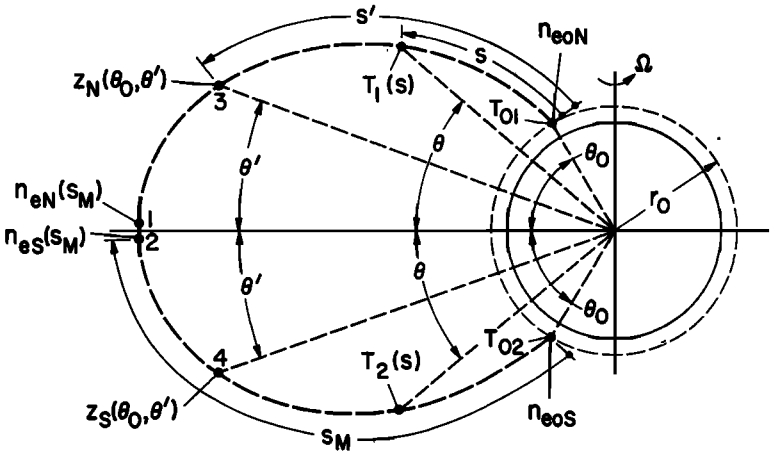

Fig. 10. The variation of temperature along a line of force. In the northern hemisphere the temperature is given by $T_1(s)$, and in the southern hemisphere by $T_2(s)$ (see Figure 11). This diagram is also pertinent to the calculation of ratios of electron densities at conjugate points, as in the next section.

(39). Also, the effect of neglecting the centrifugal force is negligible below $\theta_0 = 45°$.

It is important to note that the calculated electron distributions depend strongly on the assumed base temperature, but do not depend appreciably on the small temperature changes assumed along a line of force, and that, to a first order, vertical profiles and distributions along the line of force computed assuming a constant temperature are adequate.

To convert the relative electron density distributions to absolute values, electron density data for 1000 km obtained from the Alouette satellite were used. Figure 13 (after *Thomas and Sader* [1963]) shows the mean variation of the electron density at 1000 km for a series of magnetically quiet days and nights in summer and winter as a function of dip latitude. The broken lines are extrapolated values.

$N(h)$ equatorial profiles were then computed for a variety of conditions using the data of Figures 13 at 1000 km. If the assumptions about temperature and base compositions are correct (Table 2), the theory outlined in this paper predicts that the electron profiles in summer (day and night) are as shown in Figures 14*a* and *b*.

The differences among the curves within each

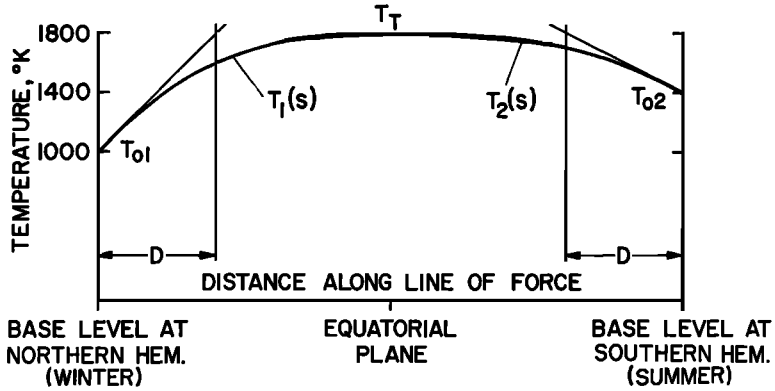

Fig. 11. The schematic variation of temperature along a line of force, as given by (40). $T_1(s)$ is used for the temperature distributions in the northern (winter) hemisphere and $T_2(s)$ for the southern (summer) hemisphere.

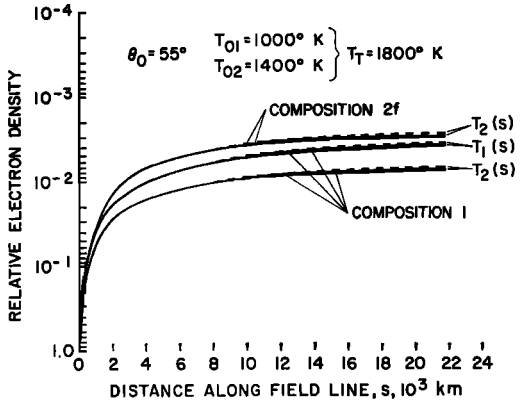

Fig. 12. The relative electron density distribution along a field line with feet (at 500 km above the earth) at geomagnetic latitude 55° (see Table 2) for a nonisothermal exosphere (see Figure 11). The broken lines indicate the distributions that would have been obtained if the centrifugal force had been neglected.

of the two figures arise because of the different assumptions about temperature and composition. The differences between the two groups of curves are due to the latitude dependence of electron density at 1000 km differing from day to night (see Figure 13). In particular, the rapid fall-off of electron density with height in the curves for summer night is attributable to the rapid decrease in the electron density at 1000 km with dip latitude over the range 50°–65°. Typical diurnal and seasonal changes are illustrated for a given temperature and base composition in Figure 15, which shows also the value of the latitude θ_0 corresponding to the foot of the field line (at 1000 km above the earth) which extends to a given distance from the center of the earth in the equatorial plane.

No *detailed* comparison of the predicted $N(h)$ profiles with experimentally observed data for any given day is possible at the present time. However, a number of whistler mean exospheric electron density profiles have been published covering a wide range of observational conditions. A number of these are reproduced in Figure 16, labeled *a* to *h* [*Storey*, 1953; *Allcock*, 1959; Carpenter and Angerami (quoted by *Carpenter*, 1963); *Smith*, 1960, 1961; *Pope*, 1961, 1962; *Schmelovsky*, 1960; *Schoute-Vanneck and Muir*, 1963]. Storey's observations are represented in the figure by a single point. *Bowles'* [1962] incoherent scatter observations lie within the range covered by the arrow.

It is interesting to compare these observations with a number of theoretical $N(h)$ distributions predicted for the exospheric plasma; these are discussed in the next section. The typical examples reproduced in Figure 17 [*Bates and Patterson*, 1961; *Dungey*, 1954; *Johnson*, 1960] can be compared with the curves predicted by the theory presented here. Curve *d*, as originally given by *Johnson* [1960], applies along a line of force and assumes H^+ only. To get the equatorial profile curve *d* of Figure 17, a constant density was assumed at the base level.

In Figure 17 the experimental observations of Figure 16 are superposed on the theoretical curves. The experimental curves of Figure 16

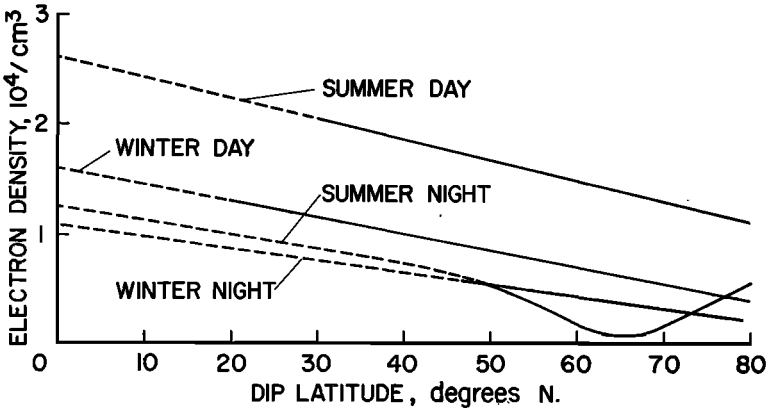

Fig. 13. The average quiet day electron density at 1000 km (after *Thomas and Sader* [1963]). The continuous lines are observed values and the broken lines are extrapolations which are roughly consistent with equatorial Alouette data.

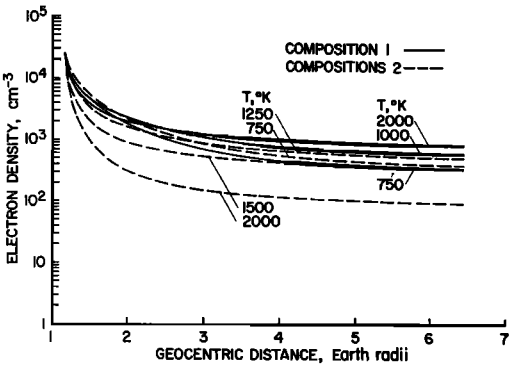

Fig. 14*a*. Theoretically predicted equatorial $N(h)$ profiles based on observed Alouette data for the electron density at 1000 km for *summer days*. Curves for a wide variety of isothermal exospheric temperatures and compositions at 500 km are illustrated (see Table 2).

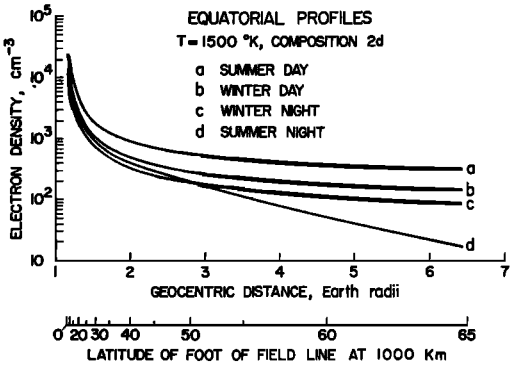

Fig. 15. Calculated equatorial electron profiles based on the electron densities measured by Alouette at 1000 km under different conditions, to show seasonal and diurnal variations. The composition at 500 km and the temperature are assumed to be constant in latitude.

cover a wide variety of observed conditions and include results for different times of day, different seasons, and different solar epochs. In general, however, all these results lie within the approximate region indicated by the dotted area in Figure 17. The values of electron density measured by Alouette lie within the approximate zone indicated by the vertically shaded area.

It is clear from Figure 17 that, when the values of electron density at 1000 km given by the Alouette data for summer nights are used, the theory outlined in this report gives reasonably good agreement with the observations (curves *e* and *f*), whereas the curves *a*, *b*, *c*, and *d* indicate too small a decrease of electron density with height. Furthermore, the present theory provides a better agreement with the observed slope of the $N(h)$ profile near the level of the Alouette orbit.

Until further information is available about the exospheric temperature and composition, it is probably unfruitful to consider detailed com-

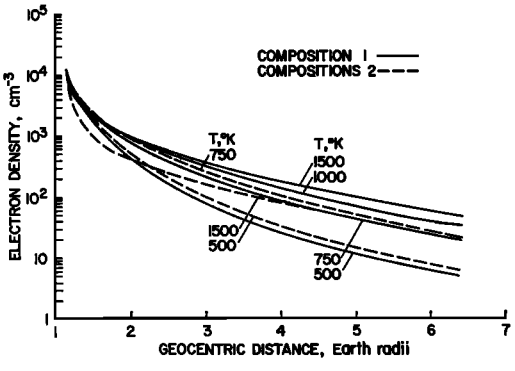

Fig. 14*b*. Theoretically predicted equatorial $N(h)$ profiles based on observed Alouette data for the electron density at 1000 km for *summer nights*. Curves for a wide variety of isothermal exospheric temperatures and compositions at 500 km are illustrated (see Table 2). Note the marked increase in the rate of fall-off of electron density with height at great distances from the earth.

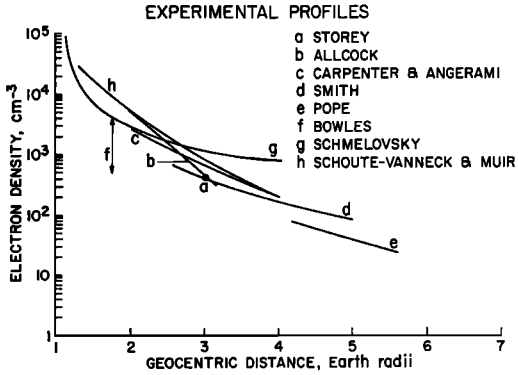

Fig. 16. Examples of measurements of electron density in the equatorial plane. The arrow *f* represents a range of values obtained by the incoherent scatter technique under different conditions. The other data (see text) come from whistler observations, also made under a wide variety of conditions (time, season, and magnetic and solar activities).

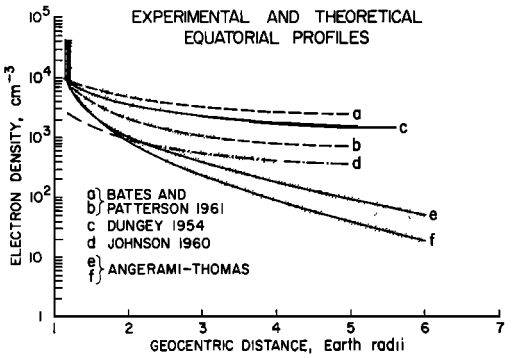

Fig. 17. Comparison of experimental and theoretical exospheric $N(h)$ profiles in the equatorial plane. The dotted area approximates the region within which the experimental profiles of Figure 16 are observed. The vertical shading near 1000 km approximates the region in which the Alouette observations for 1000 km lie. The temperatures for curves *a*, *b*, *e*, and *f* are 2000, 1000, 1500, and 750°K, respectively. Curves *e* and *f* were calculated by assuming composition 1 at 500 km, and electron density at 1000 km as measured by Alouette on summer nights (see Figure 13). Curve *d* was plotted assuming a constant electron density at the base level.

parison of theory with experiment. However, the number of reasonable choices is not unlimited; for example (Figure 18), *Smith*'s [1960, 1961] $N(h)$ curve is well matched by the present theory if the temperature is assumed to be 1000°K and the starting electron density at 1000 km is assumed to be roughly that corresponding to the curve labeled 'summer night' in Figure 13. Thus, quite good agreement can be obtained with values which might reasonably be expected to apply at the time when the whistler observations were made.

Calculation of Ratio of Electron Densities at Conjugate Points

Attention will be given now to a rather interesting consequence of the theory presented earlier, namely, the ratio R_e that must exist between the electron densities at the reference level at two magnetically conjugate points to satisfy continuity at the top of the field line.

It will be assumed that the ions and electrons have the same temperature, and hence $C = 1$ in (21).

Temperature constant in each hemisphere. As a first approximation, suppose that the average temperature in the southern (summer) hemisphere T_S is greater than the average temperature in the northern (winter) hemisphere T_N (Figure 19), so that

$$T_S = KT_N \tag{41}$$

with K a constant greater than 1.

Given the electron density n_{e0} (and ion densities, through η_2 and η_3) at a reference point on a field line, it is possible to calculate the electron density at any other point (defined by θ_0, θ') on the same field line using (34) and (B.4).

Let A be the ratio $n_e(s')/n_{e0}$ given by (34). It is clearly a function of temperature, through the values of H_i and η_i. Thus, for the northern and southern hemispheres, respectively,

$$\frac{n_{eN}}{n_{e0N}} = A_N = \left[\frac{1}{\eta_N}\sum_i \eta_{iN} \exp\left(-z_M/H_{iN}\right)\right]^{1/2} \tag{42a}$$

$$\frac{n_{eS}}{n_{e0S}} = A_S = \left[\frac{1}{\eta_S}\sum_i \eta_{iS} \exp\left(-z_M/H_{iS}\right)\right]^{1/2} \tag{42b}$$

where z_M, the value of z for $\theta' \approx 0$, is given by (B.5).

As the electron pressure must be the same in points 1 and 2 of Figure 19,

$$n_{eN}kT_N = p_N = p_S = n_{eS}kT_S$$

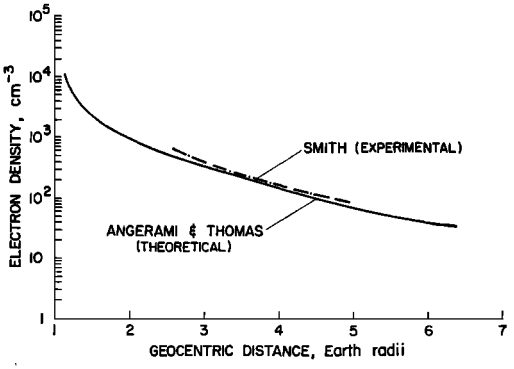

Fig. 18. Comparison of theory and experiment. The theoretical curve was computed assuming a constant exospheric temperature of 1000°K and ionic composition 1 (see Table 1) at the base level. The electron density at 1000 km was taken to be that given by Alouette for summer night conditions (see Figure 13).

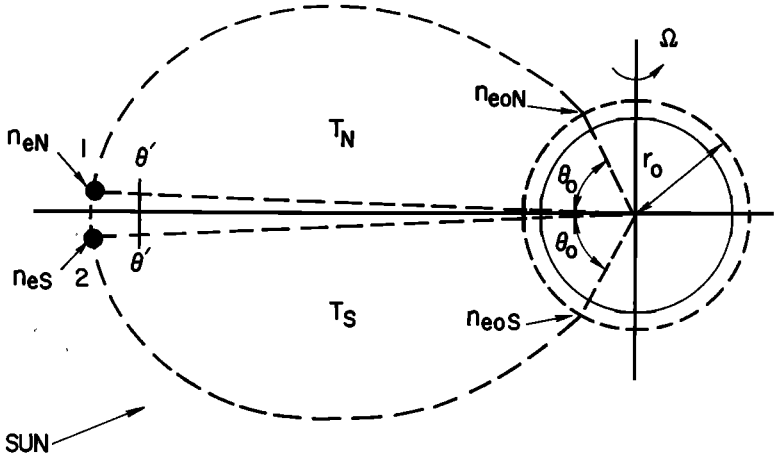

Fig. 19. Parameters used to calculate the electron density ratio R_e at the reference level at two magnetically conjugate points when the temperatures in the northern and southern hemispheres are different but constant in each hemisphere.

From these equations, and using (41) and (42), we obtain

$$R_{e0} = \frac{n_{e0N}(\theta_0)}{n_{e0S}(\theta_0)} = K\frac{A_S}{A_N}$$

This expression permits the calculation of the electron density at the reference level in the northern hemisphere if the electron density at the same level, at the conjugate point, is known. It is useful to make the following approximations.

From Figure 5 it is seen that for z greater than about 3500 km (corresponding to z_M at $\theta_0 > 40°$), (33) holds, so that with the present assumptions, using (16), A_N and A_S are given by

$$\begin{aligned} A_N &\approx \sqrt{\eta_{3N}/\eta_N}\ \exp\left(-z_M/2H_{3N}\right) \\ A_S &\approx \sqrt{\eta_{3S}/\eta_S}\ \exp\left(-z_M/2KH_{3N}\right) \end{aligned} \tag{43}$$

Thus, at latitudes greater than about 40°, we can write

$$\begin{aligned} R_{e0} &= \frac{n_{e0N}(\theta_0)}{n_{e0S}(\theta_0)} \\ &\approx K\sqrt{\frac{\eta_{3S}\eta_N}{\eta_{3N}\eta_S}}\ \exp\left(\frac{z_M}{2H_{3N}}\frac{K-1}{K}\right) \end{aligned} \tag{44}$$

The corresponding equation given by *Rothwell* [1962] can be derived as a particular case of the more general expression 44 in which the dependence of m and g on altitude can be properly allowed for.

Temperature changing along a line of force. In the preceding section, it was assumed as a convenient approximation that there was a discontinuity of temperature between two points just north and south of the equatorial plane (Figure 19). For a complete treatment, it is better to proceed as follows.

Figure 11 indicates the temperature as a function of distance along a line of force. The temperature must change along the field line, since it is supposed that, at the reference level, it has different values in the northern and southern hemispheres:

$$T_{02} = KT_{01} \tag{45}$$

with K a constant greater than 1.

The distance s in Figure 10 is clearly a function of θ_0 and θ, and we call $s_M(\theta_0)$ the value of s corresponding to $\theta = 0$ (details are given in appendix A).

The functions $T_1(s)$ and $T_2(s)$ are such that the temperature is a continuous function of s, including the point s_M; that is,

$$T_1(s_M) = T_2(s_M) = T_T \tag{46}$$

As the temperature is now a function of s, (B.3) must be used to calculate z, and different values will result for points 1 and 2 of Figure 10

$$z_N(\theta_0, 0) = r_0 \int_0^{\theta_0} \frac{T_{01}}{T_1(s)} \sin\theta \cdot \left\{ \frac{2\cos^2\theta_0}{\cos^3\theta} - \frac{3\Omega^2 r_0}{g_0} \frac{\cos^5\theta}{\cos^4\theta_0} \right\} d\theta$$

$$z_S(\theta_0, 0) = r_0 \int_0^{\theta_0} \frac{T_{02}}{T_2(s)} \sin\theta \cdot \left\{ \frac{2\cos^2\theta_0}{\cos^3\theta} - \frac{3\Omega^2 r_0}{g_0} \frac{\cos^5\theta}{\cos^4\theta_0} \right\} d\theta \quad (47)$$

These equations, together with (24), give the electron density distributions in the northern and southern hemispheres:

$$\frac{n_{eN}(s_M)}{n_{e0N}} = \frac{T_{01}}{T_1(s_M)} \cdot \left\{ \frac{1}{\eta_N} \sum_i \left[\eta_{iN} \exp\left(-\frac{z_N}{H_{iN}} \right) \right] \right\}^{1/2} \quad (48a)$$

$$\frac{n_{eS}(s_M)}{n_{e0S}} = \frac{T_{02}}{T_2(s_M)} \cdot \left\{ \frac{1}{\eta_S} \sum_i \left[\eta_{iS} \exp\left(-\frac{z_S}{H_{iS}} \right) \right] \right\}^{1/2} \quad (48b)$$

For the top of the field line the electron densities are the same in the northern and southern hemispheres (points 1 and 2 of Figure 10), and so are the temperatures. Thus, the last equations, together with (46), give

$$R_e = K \left\{ \frac{\eta_N}{\eta_S} \frac{\sum_i \{\eta_{iS} \exp(-z_S/H_{iS})\}}{\sum_i \{\eta_{iN} \exp(-z_N/H_{iN})\}} \right\}^{1/2} \quad (49)$$

where z_N and z_S are given by the corresponding equations 47. For sufficiently large values of z_S and z_N such that (33) holds, (49) can be written as

$$R_e \simeq K \left\{ \frac{\eta_N}{\eta_S} \frac{\eta_{3S}}{\eta_{3N}} \right\}^{1/2} \exp\left\{ \frac{z_{MN} - z_{MS}/K}{2H_{3N}} \right\}$$

in which (16) and (45) have been used.

The ratios R_e of the electron densities at conjugate points in the two hemispheres predicted by the theory were calculated for a series of heights (Figure 20). The temperature distribution along a line of force was assumed to be as shown in Figure 11, the temperature T_{01} corresponding to that at the base level in the northern (winter) hemisphere. The ionic composition

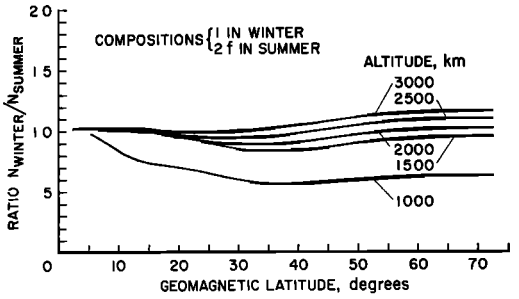

Fig. 20. The predicted ratio of the electron density in winter to that at the same location and altitude in summer for a number of different altitudes. Compositions 1 and 2f (see Table 1) are used at 500 km. The assumed temperature distribution is illustrated in Figure 11.

at 500 km was assumed to depend on the temperature as given by *Bauer* [1963] (Figure 7 and equations 39). The ratio R_e is about unity except for the 1000-km level, for which it decreases from 1 at the equator to approximately 0.5 at high latitudes (Figure 20). If it is supposed that the compositions at the base level are the same in winter and summer, the ratio R_e is slightly greater than unity and tends to increase with increasing latitude [*Angerami and Thomas*, 1963, Figure 15*a*].

The general agreement between theory and experiment is illustrated in another way in Figure 21, which shows the theoretically predic-

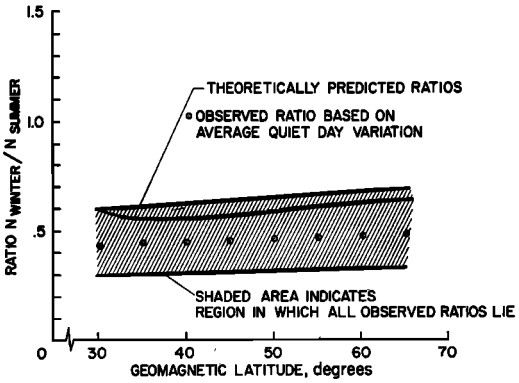

Fig. 21. Observed and predicted ratios of the electron density at 1000 km at conjugate points in the winter and summer hemispheres. The circled points, giving the observed average quiet day ratios, are based on summer and winter Alouette observations at Stanford. The ratio is approximately 0.5 over the latitude range considered. The theoretically predicted ratios are in reasonably good agreement.

ted values of the ratio R_e at 1000 km as a function of geomagnetic latitude, together with observations of R_e at 1000 km measured by the Alouette satellite. The shaded area corresponds to values within which all the observed values of the ratio R_e lie and thus allows for changes from day to day, etc. The circled points give the values for magnetically quiet days.

Discussion of Results

Slope of the $N(h)$ Profile in the Lower Exosphere (Approximately 600–1000 km)

It has been assumed in the theory that the production of electrons by the sun's ionizing radiations and the loss of electrons by recombination are both nonexistent. Thus no attempt is made to discuss the $N(h)$ distributions at or near the peak of the F_2 layer, though a great deal of observational and theoretical data are available [e.g., *Thomas*, 1963; *Rishbeth et al.*, 1963, and references therein]. Instead, the discussion has been confined to consideration of the theory which might apply above the critical level [*Johnson*, 1960] at about 500 km above the earth's surface.

Bauer [1962, 1963] assumed that in the vicinity of the Alouette orbit there is diffusive equilibrium with O^+, He^+, and H^+ as the main constituents, and later he was able to fit a topside profile from the Alouette satellite on the basis of an equilibrium theory down to quite low altitudes. The results of the theory outlined in the present work in the vicinity of the Alouette orbit agree with Bauer's.

The main difference between the work presented in this paper and Bauer's work is that he considers an isothermal case and does not allow for centrifugal force; both assumptions are justified for the cases he considers, since he restricts his theory to distances which do not exceed about one earth radii above the F_2-region peak. Bauer, however, considers equilibrium in a vertical column rather than in a column confined by a tube of force. In the approach outlined in this report, a vertical profile is very strongly influenced by a north-south gradient in the temperature and ionic composition at the base level or by a north-south gradient in the electron density at the base level.

Since the calculations described in this report were carried out, a number of $N(h)$ profiles deduced from the Alouette satellite data have been circulated [*King et al.*, 1963*a*, *b*; *Radio Research Station*, 1963]. The available profiles correspond to equatorial crossings of the satellite and were observed at the telemetry station at Singapore. From the $N(z)$ plots of *Radio Research Station* [1963], measurements were made of the scale height for electrons at 1000 km for one daytime and one nighttime revolution: November 26, 1962, 1458 local time and April 15, 1963, 2028 local time, respectively.

For the daytime pass, the scale height at 1000 km varies between 170 km at 14°N latitude (consistent with O^+ at 1380°K) and 260 km at 12°S latitude (consistent with a mixture of O^+ and He^+ at 1380°K). Around the latitude 14°N the electron distribution is a pure exponential down to 350 km, supporting the idea that O^+ is indeed strongly predominant.

For the nighttime pass, the scale height at 1000 km varies between 380 km at 20°N (consistent with strongly predominant He^+ at 780°K, or a mixture of He^+ with a significant amount of O^+ at a slightly higher temperature) and 620 km at 9°S (consistent with strongly predominant He^+ at 1270°K, or a mixture of He^+ and a significant amount of H^+ at a slightly lower temperature). The preceding measurements show then that the lower boundary of the helium layer is lower at night than during the day.

It appears that the scale height for electrons at 1000 km varies strongly from day to night (by a factor of 2.4 in the above measurements) and also varies with latitude. It is apparent that, at 1000 km, both the ionic composition and the temperature must vary diurnally and also with latitude, at least in the equatorial regions. Also, it is important to note that the assumption that H^+ strongly predominates at 1000 km would necessitate extremely low temperatures to explain scale heights as low as 170 km.

It should be noted that the slopes of the profiles near 1000 km for curves *a*, *b*, *c*, and *d* in Figure 17 are not in agreement with those observed from electron density profiles deduced in the vicinity of the Alouette orbit. The theoretical profiles of *Dungey* [1954], *Bates and Patterson* [1961], and *Johnson* [1960] allow only for the presence of H^+ and not for helium or oxygen. Thus, the slopes are small even at

low altitudes. The present work produces slopes in agreement with those observed by the Alouette satellite near its orbit, in conformity with the results of Bauer.

Slope of the $N(h)$ Profile in the Upper Exosphere

An examination of the theoretical profiles of Figure 17 shows that at very great heights the rate at which the electron density decreases with height is often less than the experimental observations indicate.

On the basis of hydrostatic support, if the exosphere above 1000 km is composed of H^+ only (or if the ionic composition at that level is assumed constant with latitude), the equatorial electron profiles of Figure 16 can be explained only by a latitude dependence of the electron density at 1000 km, as is the case for curves *e* and *f* in Figure 17.

It must be emphasized that agreement between the experimental data of Figure 16 and an approximately constant electron density at the base level (as shown in Figure 11, except the curve labeled 'summer night') is still possible under the assumption of hydrostatic support if the ionic composition at 1000 km changes properly with latitude. The required variation is such that at higher latitudes the light constituents are less abundant.

At the present time, neither the ionic compositions at 1000 km nor the exospheric temperature as a function of latitude is known, and no further comments can be safely made. It is expected that possibilities for the ranges of composition and temperature at 1000 km will be narrowed by measurements, which will be available soon, on $N(h)$ profiles determined by Alouette over a wide range of latitudes.

At the present time, until more information is available about the positive ion abundances at 1000 km, it is not known to what extent profiles observed at all times can be fitted by a simple equilibrium theory. However, it is clear that the main features of the seasonal variations will probably, to a large extent, be governed by the broad precepts dictated by an equilibrium theory, although there will be diurnal changes superimposed on the seasonal changes. The theory outlined in this paper does, under certain circumstances, lead to electron density profiles which fall off at great altitudes at a rate which is in agreement with the experimental data obtained from whistlers and at the same time gives the correct slope near the Alouette orbit.

Conclusions

1. The equations describing the equilibrium distributions of electrons and ions in a planetary exosphere have been presented. Computations have been made for the earth's exosphere for a wide variety of conditions on the assumption that diffusive equilibrium applies.
2. The theory assumes that diffusion of electrons and ions is possible only along the magnetic field lines.
3. The presence of He^+ ions near the base of the exosphere has been allowed for in the calculations. This is vital for an understanding of the changes accompanying the transition from day to night conditions.
4. The most crucial factors governing the form of these distributions are the exospheric temperature and the ionic composition at the base level, assumed to be at 500 km above the earth's surface.
5. The latitude dependence of electron density at 1000 km, as observed by the Alouette satellite, has been taken into consideration in the calculations. As a result, it is clear that the discrepancy previously observed between theory and experiment, namely, that the electron density gradient at great heights predicted by the theories turned out to be much smaller than that indicated by the whistler observations, is now removed under certain circumstances.
6. The effect of the earth's centrifugal force is included in the calculations; its neglect would, at the high altitudes, lead to electron density values that are too low at a given height by an amount which does not exceed 20% for altitudes less than about 6 earth radii.

Although it is not suggested that an equilibrium theory is adequate to describe the entire properties of the plasma distribution in the exosphere, it is quite clear that a first-order agreement can be obtained, at any rate, in terms of seasonal dependencies. The basic question of why the electron density at the Alouette orbit varies with latitude in the way that it does remains unsolved. Further work is needed to determine the nature and the relative abun-

dances of the positive ions at the base of the exosphere and the dependence of these relative abundances on the exospheric temperatures. Measurements of the relative abundances on a daily routine basis through satellite observations will probably be necessary before it is possible to determine accurately the circumstances in which an equilibrium theory becomes inapplicable.

Appendix A

Geometry of the Dipole Field

It was assumed in this report that the actual magnetic field of the earth could be approximated by a centered dipole field, as indicated in *Mlodnosky and Helliwell* [1962]. Most of the equations quoted in this appendix appear in Figure 1 of their paper, to which reference should be made. Thus, the equation of a line of force in a dipole field is

$$r/r_0 = \cos^2 \theta / \cos^2 \theta_0 \qquad (A.1)$$

in which the quantities are as shown in our Figure 1. In the figure, the distance s_1 along the line of force with feet at θ_0, from the equatorial plane to the latitude θ, is

$$s_1(\theta_0, \theta) = \frac{r_0}{2\sqrt{3}\cos^2 \theta_0}(x + \sinh x \cdot \cosh x)$$

$$= \frac{r_0}{2\sqrt{3}\cos^2 \theta_0}[\ln (y + \sqrt{1 + y^2}) + y\sqrt{1 + y^2}] \qquad (A.2)$$

where

$$y = \sinh x = \sqrt{3} \sin \theta$$

We called $s_M(\theta_0)$ the value of s_1 corresponding to $\theta = \theta_0$, as shown in Figure 10:

$$s_M(\theta_0) = \frac{r_0}{2\sqrt{3}\cos^2 \theta_0} \cdot [\ln (y_0 + \sqrt{1 + y_0^2}) + y_0\sqrt{1 + y_0^2}] \qquad (A.3)$$

with

$$y_0 = \sqrt{3} \sin \theta_0$$

For convenience, the distance $s(\theta_0, \theta)$ between a base level (θ_0) and a latitude θ was used (Figure 1):

$$s(\theta_0, \theta) = s_M(\theta_0) - s_1(\theta_0, \theta) \qquad (A.4)$$

The increment of distance ds, corresponding to an increment $d\theta$ (keeping θ_0 constant), is easily shown to be

$$ds = -\frac{r_0}{\cos^2 \theta_0}\sqrt{1 + 3 \sin^2 \theta} \cos \theta \, d\theta \qquad (A.5)$$

It is clear that by means of (A.1) the distances s_1, s_M, and s can be written as functions of (θ_0, r), and this is convenient for electron and ion density calculations in which the exospheric temperature is assumed constant. This procedure was used in the computations leading to Figures 9, 14, and 15.

It should be noted that the inversion of (A.2) or (A.4) to give θ as a function of θ_0 and s_1 (or s) is only possible numerically. Thus, in the computations leading to Figures 12 and 20, in which the temperature is assumed to be a function of the distance s, the numerical integrations to get z (from (B.3)) were made using θ as the independent variable.

Appendix B

Calculation of Temperature-Modified Geopotential Height z

It will be recalled that the quantity z (equation 14) is defined by

$$z(\theta_0, s') = \int_0^{s'} \frac{f(\theta_0, s)}{g_0} \frac{T_{e0}}{T_e(s)} ds \qquad (B.1)$$

To evaluate z it is necessary to transform the variable of integration in the above equation from s to θ, where θ is the geomagnetic latitude of the point concerned on the line of force. In appendix A, it is shown that the element of distance ds along the line of force can be written in terms of the subtended angular increment $d\theta$ by the relationship

$$ds = \frac{-r_0}{\cos^2 \theta_0} \cos \theta \sqrt{1 + 3 \sin^2 \theta} \, d\theta \qquad (B.2)$$

Substituting for ds from (B.2) and for f from (4) in the above expression for z and using (A.4), we have

$$z = r_0 \int_{\theta'}^{\theta_0} \frac{T_{e0}}{T_e(\theta)} \sin \theta \cdot \left\{\frac{2 \cos^2 \theta_0}{\cos^3 \theta} - \frac{3\Omega^2 r_0 \cos^5 \theta}{g_0 \cos^4 \theta_0}\right\} d\theta \qquad (B.3)$$

This expression for z, the temperature-modified geopotential height, if substituted into (21) and (23), will give the density distribution of electrons and ions *along a line of force* for any given temperature distribution along a line of force. In general, the equation will have to be computed numerically on a digital computer. In the case of a constant temperature along a line of force, so that $T_e(\theta) = T_{e0}$, we have

$$z(\theta_0, \theta') = r_0\left\{\left[1 - \frac{\cos^2 \theta_0}{\cos^2 \theta'}\right] + \frac{\Omega^2 r_0}{2g_0}\left[\cos^2 \theta_0 - \frac{\cos^6 \theta'}{\cos^4 \theta_0}\right]\right\} \quad \text{(B.4)}$$

so that, in the simple case of an isothermal atmosphere, z has an analytical solution.

The resultant variation of z with altitude is shown in Figure 4 for different latitudes. If the centrifugal force is disregarded, z is a function of altitude only and is independent of latitude (curve at right). It approaches a limiting value (equal to the distance from the reference level to the center of the earth) as the altitude goes to infinity. Inclusion of the centrifugal force implies a decrease in z, especially at high altitudes and low latitudes. The quantity z then has a maximum value at approximately six earth radii for low latitudes and approximately eight earth radii for higher latitudes.

It should be noted, of course, that in (21) and (23) it is possible for the temperature along different lines of force to be different and to be distributed along each line of force in a different way. As stated above, (21) and (23), in conjunction with the general relationship (B.3), can be used to compute the profile of electron density along a line of force. If, however, only the ratio of electron densities in the northern and southern hemispheres at the base level is required (see section Calculation of Ratio of Electron Densities at Conjugate Points), then it is useful to consider the form of (B.4) when θ' is small, so that the point (θ_0, θ') lies near the equatorial plane. For $\theta' \approx 0$ the value z_M of z from (B.4) becomes

$$z(\theta_0, \theta') = z_M(\theta_0) = r_0\left\{[1 - \cos^2 \theta_0] + \frac{\Omega^2 r_0}{2g_0}\left[\cos^2 \theta_0 - \frac{1}{\cos^4 \theta_0}\right]\right\} \quad \text{(B.5)}$$

Acknowledgments. We acknowledge valuable discussions with Professors R. A. Helliwell and O. K. Garriott.

The main part of this work was carried out while one of us (J. O. Thomas) was a Visiting Scientist at Stanford University. The interest and cooperation of Professor O. G. Villard and colleagues in the Radioscience Laboratory, Stanford Electronics Laboratories, Stanford University, is gratefully acknowledged.

One of us (J. J. Angerami) wishes to acknowledge support from the Escola Politecnica, University of São Paulo, Brazil.

The work was financed in part by grant NsG 30-60 from the National Aeronautics and Space Administration and in part by the Air Force Office of Scientific Research under grant AF-AFOSR-62-370.

References

Allcock, G. M., The electron density distribution in the outer ionosphere derived from whistler data, *J. Atmospheric Terrest. Phys., 14,* 185, 1959.

Angerami, J. J., and J. O. Thomas, The distribution of ions and electrons in the earth's exosphere, *Stanford Electron. Lab. Tech. Rept. 4, NASA grant NsG 30-60,* and *Tech. Rept. 3412-3, grant AF-AFOSR-62-370, Stanford Univ.,* 1963.

Bates, D. R., and T. N. L. Patterson, Hydrogen atoms and ions in the thermosphere and exosphere, *Planetary Space Sci., 5,* 257, 1961.

Bauer, S. J., On the structure of the topside ionosphere, *J. Atmospheric Sci., 19,* 276, 1962.

Bauer, S. J., Helium ion belt in the upper atmosphere, *Nature, 197,* 36, 1963.

Bordeau, R. E., Rocket and satellite investigations of the ionosphere (abstract), *Trans. Am. Geophys. Union, 44,* 443, 1963.

Bowles, K. L., Profiles of electron density over the magnetic equator obtained using the incoherent scatter technique, *NBS Rept. 7633,* 1962.

Carpenter, D. L., Whistler measurements of the equatorial profile of magnetospheric electron density, paper presented at the 14th General Assembly of URSI, Tokyo, 1963 (to be published by Elsevier Publishing Company, Amsterdam).

Dungey, J. W., Electrodynamics of the outer atmosphere, *Sci. Rept. 69, contract AF 19(122)-44, Ionospheric Res. Lab., Penn. State Univ.,* 1954.

Dungey, J. W., Electrodynamics of the outer atmosphere, in *The Physics of the Ionosphere,* p. 229, The Physical Society, London, 1955.

Gliddon, J. E. C., The distribution of ions in the exosphere, *J. Atmospheric Terrest. Phys., 25,* 175, 1963.

Hanson, W. B., Upper atmosphere helium ions, *J. Geophys. Res., 67,* 183, 1962.

Hanson, W. B., and I. B. Ortenburger, The coupling between the protonosphere and the normal F region, *J. Geophys. Res., 66,* 1425, 1961.

Hanson, W. B., and T. N. L. Patterson, Diurnal variation of the hydrogen concentration in the exosphere, *Planetary Space Sci., 11,* 1035, 1963.

Hanson, W. B., T. N. L. Patterson, and S. S. Degaonkar, Some deductions from a measurement of the hydrogen ion distribution in the high atmosphere, *J. Geophys. Res., 68,* 6203, 1963.

Harris, Isadore, and Wolfgang Priester, Theoretical models for the solar-cycle variation of the upper atmosphere, *NASA Goddard Space Flight Center X-640-62-70,* June 1962.

Johnson, F. S., The ion distribution above the F_2 maximum, *J. Geophys. Res., 65,* 577, 1960.

Johnson, F. S., *Physics of the Distribution of Ionized Particles in the Exosphere,* NATO Conference Series, vol. 2, edited by B. Maehlum, p. 404, Pergamon Press, London, 1962.

King, J. W., D. Eccles, P. A. Smith, P. Dannahy, A. Legg, E. O. Olatunji, K. Rice, G. Webb, and M. Williams, Further studies of the topside ionosphere based on the topside sounder satellite data, *D.S.I.R. Doc. I.M. 112,* Slough, 1963*b*.

King, J. W., P. A. Smith, D. Eccles, and H. Helm, The structure of the upper ionosphere as observed by the topside sounder satellite, Alouette, *D.S.I.R. Doc. I.M. 94,* Slough, 1963*a*.

King-Hele, D. G., and D. M. C. Walker, Variation of upper atmosphere density with altitude and season: Further evidence from satellite orbits, *Nature, 185,* 727, 1960.

Mange, P., The distribution of minor ions in electrostatic equilibrium in the high atmosphere, *J. Geophys. Res., 65,* 3833, 1960.

Mlodnosky, R. F., and R. A. Helliwell, Graphic data on the earth's main magnetic field in space, *J. Geophys. Res., 67,* 2207, 1962.

Nicolet, M., Helium, an important constituent in the lower exosphere, *J. Geophys. Res., 66,* 2263, 1961.

Pope, J. H., An estimate of electron densities in the exosphere by means of nose whistlers, *J. Geophys. Res., 66,* 67, 1961.

Pope, J. H., A correction to the exospheric electron density estimate using the nose whistlers of March 19, 1959, *J. Geophys. Res., 67,* 412, 1962.

Radio Research Station, *Height Distribution of Electron Concentration in the Topside Ionosphere As Deduced from Topside Sounder Satellite Ionograms, Vol. 1,* D.S.I.R., Slough, 1963.

Rishbeth, H., A. J. Lyon, and M. Peart, Diffusion in the equatorial *F* layer, *J. Geophys. Res., 68,* 2559, 1963.

Rothwell, P., Diffusion of ions between *F* layers at magnetic conjugate points, *Proc. Intern. Conf. Ionosphere,* p. 217, The Institute of Physics and The Physical Society, London, 1962.

Schmelovsky, K. H., The electron density distribution derived from whistler data and Faraday-fading observations, *J. Atmospheric Terrest. Phys., 19,* 68, 1960.

Schoute-Vanneck, C. A., and M. S. Muir, The electron density distribution in the magnetosphere derived from whistling atmospheric data, *J. Geophys. Res., 68,* 6079, 1963.

Smith, R. L., The use of nose whistlers in the study of the outer ionosphere, *Stanford Electron. Lab. Tech. Rept. 6, contract AF18(603)-126, Stanford Univ.,* 1960.

Smith, R. L., Properties of the outer ionosphere deduced from nose whitlers, *J. Geophys. Res., 66,* 3709, 1961.

Storey, L. R. O., An investigation of whistling atmospherics, *Phil. Trans. Royal Soc. London, A, 246,* 113, 1953.

Thomas, J. O., The electron density distributions in the F_2 layer of the ionosphere in winter, *J. Geophys. Res., 68,* 2707, 1963.

Thomas, J. O., and A. Y. Sader, Alouette topside soundings monitored at Stanford University, *Stanford Electron. Lab. Tech. Rept. 6, NASA grant NsG 30-60, Radiosci. Lab., Stanford Univ.* 1963.

Thomas, J. O., and A. Y. Sader, The electron density at the Alouette orbit, *J. Geophys. Res., 69*(19), October 1, 1964.

(Manuscript received July 13, 1964.)